# NJC

## Accepted Manuscript

This article can be cited before page numbers have been issued, to do this please use: A. Mishura, A. S. Lytvynenko, K. S. Gavrilenko, A. E. Baranchikov, N. V. Grabovaya, M. A. Kiskin and S. V. Kolotilov, *New J. Chem.*, 2018, DOI: 10.1039/C8NJ03460E.


This is an Accepted Manuscript, which has been through the Royal Society of Chemistry peer review process and has been accepted for publication.

Accepted Manuscripts are published online shortly after acceptance, before technical editing, formatting and proof reading. Using this free service, authors can make their results available to the community, in citable form, before we publish the edited article. We will replace this Accepted Manuscript with the edited and formatted Advance Article as soon as it is available.

You can find more information about Accepted Manuscripts in the author guidelines.

Please note that technical editing may introduce minor changes to the text and/or graphics, which may alter content. The journal's standard Terms & Conditions and the ethical guidelines, outlined in our author and reviewer resource centre, still apply. In no event shall the Royal Society of Chemistry be held responsible for any errors or omissions in this Accepted Manuscript or any consequences arising from the use of any information it contains.

View Article Online
DOI: 10.1039/C8NJ03460E



# Formation of hierarchically-ordered nanoporous silver foam and its electrocatalytic properties in reductive dehalogenation of organic compounds

Andrey M. Mishura,[†] Anton S. Lytvynenko,[†]* Konstantin S. Gavrilenko,[‡,¥] Alexander E. Baranchikov,[§] Natalia V. Grabovaya,[†] Mikhail A. Kiskin,[§] Sergey V. Kolotilov[†]

[†] L. V. Pisarzhevskii Institute of Physical Chemistry of the National Academy of Sciences of the Ukraine, Prosp. Nauky 31, Kiev, 03028, Ukraine
Tel.: +38(044)5254228; Fax: +38(044)5256216
E-mail: anton.s.lytvynenko@gmail.com

[‡] Research-And-Education ChemBioCenter, National Taras Shevchenko University of Kyiv, Chervonotkackaya str., 61, 03022, Kiev, Ukraine. E-mail: kgavrio@gmail.com

[¥] Enamine Ltd, A. Matrosova str. 23, Kiev 01103, Ukraine

[§] N. S. Kurnakov Institute of General and Inorganic Chemistry, Russian Academy of Sciences, Leninsky Prosp. 31, 119991 Moscow, GSP-1, Russian Federation
Tel.: +7(495)9522084; Fax: +7(495)9541279
E-mail: m_kiskin@mail.ru

**Abstract**

Nanoporous silver foam on glassy carbon electrode (AgNF/GC) was formed by cathodic deposition of silver from acidic solution of $AgBF_4$ at high current density. The material can be described (basing on results of optical microscopy, SEM, TEM and XRD investigation) as hierarchically (micro/nano) porous matter with *ca*. 40 nm silver crystals assembled in irregular *ca*. 70–300 nm thick filaments arranged in foam-like structure with *ca.* 20 μm cavities and *ca.* 7 μm walls. AgNF surface area was estimated by pseudocapacitance measurement as *ca*. 12 times higher than the geometrical area. Reduction of bromobenzene and other aryl bromides containing redox-inactive (F-, $CH_3$-, $CH_3O$-) or redox-active (-$NO_2$, -CN and $CH_3CO$-) substituents, as well as alkyl bromides ($CF_3CHClBr$, $CF_2Br_2$) on AgNF/GC was studied. The peaks potentials of the processes assigned to debromination of the organic halides were less negative (up to +345 mV) than on smooth silver, indicating superior electrocatalytic properties of the nanoporous silver foam. Comparison of the CV peaks currents of the processes on AgNF/GC and smooth silver, as well as their changes on cycling in different regimes allowed to suggest formation of a few kinds of electrocatalytically active sites on AgNF surface. Electrolysis of 1-bromo-4-fluorobenzene on AgNF electrode led to fluorobenzene, less than 1 mg of AgNF revealed performance comparable to 500 mg of smooth silver wire. The results can

View Article Online
DOI: 10.1039/C8NJ03460E

be utilized for creation of electrochemical sensors as well as for preparative detoxification of halogen-containing persistent organic pollutants.

**Keywords:**

Nanoporous metal foam, silver, reductive dehalogenation, electrocatalysis, organic halides, persistent organic pollutants, DFT



## Introduction

Metal nanoparticles and nanostructures are widely used as catalysts of various organic reactions[1,2], for example, new C-C, C-N bonds formation[3–6], hydrogenation[7], oxidation[8,9]. Various nanostructures have high potential of use in medicine[10,11], sensorics[12], *etc.* Silver nanoparticles and composite nanostructures are considered as promising catalysts of diverse reactions[13,14]. In particular, Ag-containing nanosized species showed catalytic activity in reductive processes, such as selective hydrogenation [15–18], electrocatalytic dehalogenation of chloroform [19,20], pesticides[21], as well as in oxidative processes, for example, epoxidation of alkenes [8,22]. Nanoporous silver was shown to be catalytically active in oxidation of organosilanes[23]. Silver nanoparticles could also catalyze non-redox transformations, such as phenolysis of epoxides [24]. It was shown that catalytic activity of nanomaterials depends on the particles size and material's topology [25–27]. Hence, catalytic activity of silver nanoparticles or nanostructured material can be very different from the properties of bulk silver. Development of methods for creation of new Ag nanostructures and studies of the influence of their structure on chemical properties is one of the hot topics of modern physical chemistry, catalysis and materials science.

Nanoporous metal foams[28] (NMFs, sometimes also referred as metal nanofoams[29]) can be defined as three-dimensional structures comprised of metallic particles (or filaments) interconnected in such way that leads to formation of interparticle sub-micron pores which significantly contribute to overall surface area of the foam.[28] This class of nanoscaled materials can combine useful properties of nanosized metal forms (such as high specific surface, catalytic activity *etc.*) with properties of bulk metals[28] (such as mechanical strength, high electrical and thermal conductivity). Additionally, contrary to *e.g.* nanoparticles and nanotubes, a sample of nanoporous metal foam is a unitary whole, can be used without additional binding or supporting materials in many cases and can be formed by electrochemical deposition on hardly accessible surfaces, such as interior of conducting tubes, which is important for some applications (in particular, flow reactors). Nanoporous copper,[30,31] iron,[31] silver,[32–35] gold,[36,37] palladium,[38] platinum[39] *etc.* as well as alloys (Ag-Pd[33] and Cu-Ni[40] *etc.*) were previously reported. Such materials are considered to be promising[28] for supercapacitors, batteries, hydrogen storage,

View Article Online
DOI: 10.1039/C8NJ03460E



antimicrobial scaffolds, heat sinks, catalysts and electrocatalysts *etc.* Despite that, NMFs are relatively scarcely studied, and a noticeable part of the publications devoted to these objects describe only synthesis and structure of the foams but not their properties.

Nanoporous metal foams can be prepared in the variety of ways, including chemical decomposition of metal complexes with nitrogen-rich energy-rich ligands such as *bis*(tetrazolato)amine[31] or cyanamide[41] (foaming is achieved by intense evolution of gaseous nitrogen), chemical[34] or electrochemical[42] dealloying as well as by electrodeposition of metal from solution of its salt or coordination compound under high current density concurred with hydrogen evolution.[30,43] The latter approach attracts especial interest due to its relative technical simplicity and formation of readily available electrodes in its result.

This combination of properties attracts especial attention for electrocatalytic applications, as nanoporous metal foam sample can serve as electrode with catalytically active surface.[30] Nanoporous metal foams were shown to be electrocatalytically active in $CO_2$ reduction (to formic acid or carbon monoxide on Cu[30] and Ag[34,35] foams, respectively), oxygen reduction reaction (Pd[38] foam), $CCl_3COOH$ dechlorination (Ag[33] foam) *etc.* These materials revealed superior electrocatalytic activity with respect to the corresponding bulk metals as in terms of significant cyclic voltammetry peak potential shift[33] or current difference at the same potential in chronoamperometic experiment[34] as well as in terms of increased faradaic efficiency in bulk electrolysis.[30,34,35]

A variety of halogenated organic compounds (such as chloroform, DDT, freons, polychlorinated biphenyls *etc.*), especially applied as insecticides, fungicides and pesticides, are relatively inert environmental pollutants.[44] Reactions of their electrochemical reduction attract attention as a convenient way to detect[45] and destruct[44] them as well as convert them to valuable functionalized compounds such as carboxylic[46,47] or sulfinic[47] acids (including halogen-containing ones). Potentials of these processes significantly depend on cathode material[48–51] which in the case of metal cathodes can be explained by high barrier of halide atom elimination accompanied by different affinity of the cathode materials to the leaving halide anion. Materials able to facilitate organic halides reduction (thus, manifesting electrocatalytic effect in these reactions) are desirable for practical applications as they can improve energy efficiency of the processes, reduce the quantity of by-products, improve characteristics of the electrochemical sensors and, in some cases, make possible to provide the entire process if the reaction is obstructed by reduction of other species present in the electrochemical cell such as solvent or even other reagents (*e.g.* $CO_2$[46]).

Silver was shown to be an iconic electrocatalyst for organic halides electroreduction.[48,51,52] Nanostructured forms of silver can be considered as the further possible

View Article Online
DOI: 10.1039/C8NJ03460E



improvement of the cathodic materials for these processes[33,45,53,54] due to probable more pronounced electrocatalytic effect or due to more efficient use of expensive silver (nanostructured silver on inexpensive support, *e.g.* activated carbon, has higher specific surface that bulk silver, and consumption of silver metal can be significantly reduced compared to bulk silver electrodes at the same efficiency).

The aim of this work was to evaluate the performance of nanoporous silver foam (AgNF) prepared by cathodic electrodeposition of silver in electrochemical reduction of organic halogen-containing substances of various structures and to compare the characteristics of the foam with the appropriate characteristics of bulk (smooth) silver.

In this work we carried out thorough study of the structure, electrochemical and electrocatalytic properties of Ag nanofoam, prepared by modification of reported method – cathodic deposition of silver in conditions, providing for hydrogen bubbles formation, supposed to be templates for foam formation. It was shown that Ag nanofoam was catalytically active in substituted bromobenzenes dehalogenation, and the potentials of such processes were shifted to positive values compared to bulk silver.

## Experimental

Analytical grade commercially available reagents (Sigma-Aldrich, Fluka) were used without further purification unless specified below. DMF was purified by stirring over $CaH_2$ followed by vacuum distillation[55]. Tetrabutylammonium tetrafluoroborate ($Bu_4NBF_4$) was recrystallized from isopropyl alcohol.

### *Synthesis of $AgBF_4$.*

$AgBF_4$ was synthesized according to a modified procedure reported earlier for $CF_3CO_2Ag$ [56]. Solution of NaOH (6.6 g, 0.16 mol) in 200 mL of distilled water was added to the solution of $AgNO_3$ (27.4 g, 0.16 mol) in 50 mL of distilled water. The precipitated $Ag_2O$ was filtered and washed with distilled water until pH of the filtrate became neutral. Wet precipitate was suspended in minimal amount of distilled water. 35 % aqueous $HBF_4$ was added to the suspension until the precipitate completely dissolved and the pH of the mixture became acidic (*ca.* 40 ml or 0.16 mol $HBF_4$). The resulted solution was filtered and dried *in vacuo*. Yield *ca.* 75 % (23.3 g, highly hygroscopic solid).

### *Preparation of glassy carbon plates coated by AgNF (AgNF/GC).*

AgNF/GC samples used in this work were prepared by cathodic electrodeposition of silver onto glassy carbon (GC) electrodes (disk with 2 mm diameter or plates of various squares) in 2-electrode cell in galvanostatic mode by adaptation of previously reported general route [43] and modification of reported method.[32] The electrochemical bath contained 0.01 M of $AgBF_4$

View Article Online
DOI: 10.1039/C8NJ03460E



and 2 M of $HBF_4$, current density equal to 3 A/cm$^2$ was applied for 60 sec using ELINS P8-S or PI-50-1.1 potentiostat. After that, the electrode was washed by immersion into distilled water, then in isopropyl alcohol and dried on air. This method allowed covering *ca.* 1 cm$^2$ of GC by AgNF.

In order to prepare large GC plate covered by AgNF a stepwise procedure was applied for maintenance of high current density. On each step the electrodeposition procedure was performed only on the part of the plate, the rest of the plate (including the back side and the edges) was kept over the bath or was covered by molten paraffin. After the end of the whole procedure as well as between the steps paraffin was removed by dissolution in *n*-heptane. Both clean and nanofoam-coated GC surface could be treated in this way, limiting electrochemically accessible surface to the part of the plate that remained free from paraffin. It should be noted, that it was not strictly necessary to cover the part of the GC plate, if it remained above the $AgBF_4$ solution, however we decided to protect the plate which was immediately above the solution in order to avoid uncontrolled contact of solution with electrode due to surface tension effects or due to inaccurate immersion of the plate into the $AgBF_4$ solution.

Mass of the nanofoam was estimated by weighting with Sartorius 4431 microbalance. For this a sample of the silver nanofoam was deposited onto a half of 6×6 mm GC plate (18 mm$^2$), while the rest of the surface, the backside and border of the plate were covered by paraffin. After washing out the paraffin with *n*-heptane and drying the sample, the silver deposit was carefully scratched out by a degreased brand new box cutter blade onto a small piece of aluminium foil used as the tare.

***Cyclic voltammetry***

Cyclic voltammetry (CV) experiments were provided using ELINS P8-S potentiostat in three-electrode electrochemical cell in argon atmosphere. 0.1 M $Bu_4NBF_4$ in DMF was used as working solution. A GC disk, a silver disk and a GC disk coated by nanoporous silver foam (diameters of the electrodes were equal to 2 mm in all cases) were used as working electrodes. A glassy carbon rod was used as a counter electrode, a silver chloride electrode filled with saturated KCl solution was used as the reference (the experimentally measured potential of the ferrocenium-ferrocene ($Fc^+$/Fc) couple *vs* this electrode under the same conditions was equal to +515 mV). CV scan rate was equal to 100 mV/s unless specified otherwise.

***Preparative electrolysis***

Electrolysis was performed in three-electrode electrochemical cell in potentiostatic mode using ELINS P8-S potentiostat. 100 mg of $Bu_4NBF_4$ and 100 μL of 1-bromo-4-fluorobenzene was dissolved in 5 mL of DMF, the solution was degassed by argon flow in the cell and than the cell was sealed. AgNF/GC was used as the working electrode. In order to prepare AgNF/GC for

View Article Online
DOI: 10.1039/C8NJ03460E



this experiment, we took 10x50 mm GC plate and covered its surface by paraffin leaving uncovered a 10×3 mm "window" and separate "window" for connection to the circuit. AgNF was deposited onto GC limited to the open "window" as described above. The paraffin was washed out, and the resulting plate was immersed into the working solution by ca. 5 mm. A magnesium plate (activated immediately before the experiment by immersion into diluted hydrochloric acid followed by immersion into distilled water and isopropyl alcohol and rapid sponging by filter paper) was used as a sacrificial anode; the silver chloride electrode (the same as described above) was used as the reference. After the electrolysis, 600 μL of the resulting solution was mixed with 200 μL of DMSO-$d_6$, 7.7 mg (one drop) of hexafluorobenzene (used as internal reference) and the mixture was investigated by $^{19}$F-NMR spectroscopy. Similar procedure was used for electrolysis in control experiments, where GC and bulk Ag were used as cathodes.

***NMR spectroscopy***

NMR spectra were measured using Varian Unity Plus 400 spectrometer.

***Measurement of the nanofoam specific surface area***

Specific surface area of AgNF/GC was compared to specific surface area of smooth silver electrode by determination of pseudo-capacitance of the above mentioned 2 mm nanofoam-coated GC disk electrode (and 2 mm silver disk electrode for comparison) by the means of cyclic voltammetry similar to the previously reported method[57] using 0.1 M $Bu_4NBF_4$ in DMF instead of 0.1 KF in water as the electrolyte. Briefly, cyclic voltammograms at various scan rates were measured in the potential range where no faradaic processes take place (Fig. S1 in Supporting Information). Cathodic currents at some arbitrary potential $E_{ms}$ ($E_{ms}$ = –200 mV was chosen in this work) within this area depended linearly on the scan rate, and the slope of this dependence was proportional to surface area of the electrode.

***Optical microscopy***

Optical microscopy studies were performed and the corresponding microphotographs were shot using XY-B2 trinocular microscope (Ningbo Sunny Instruments Co., Ltd., China) equipped with Canon PowerShot G6 camera. The camera was controlled manually or using the remote capture option (by libgphoto2 library controlled by Gimp software). The reflected light illumination of the samples was ensured with an externally mounted household 15 W LED lamp (1500 lm, 4100 K colour temperature, manufacturer – "220" LLC, Ukraine).

***Scanning electron microscopy***

Microstructure of the samples was studied using Carl Zeiss NVision 40 scanning electron microscope (micrographs were obtained at 7 kV acceleration voltage) equipped with Oxford Instruments X-MAX energy-dispersive X-ray (EDX) analyzer operating at 20 kV acceleration

View Article Online
DOI: 10.1039/C8NJ03460E



voltage installed in the Joint Research Centre of IGIC RAS. The samples were not specially prepared (in particular, they were not coated with conducting material) for SEM measurements. EDX analysis was performed in the mapping mode. Before the analysis, the samples were coated with 5 nm Au/Pd layer.

***Transmission electron microscopy***

TEM experiment was carried out on SELMI PEM-125K instrument operating at 100 kV acceleration voltage. Sample of silver nanofoam was scraped away from glassy carbon by stainless steel spatula into a microcentrifuge tube and dispersed in isopropyl alcohol by ultrasonication. A drop of the resulted suspension was dropped onto 3 mm carbon-coated copper mesh (Sigma-Aldrich), dried on air and put into the microscope.

***X-ray diffraction measurements***

X-ray powder diffraction was measured on Bruker D8 ADVANCE diffractometer using CuKα radiation (λ = 1.54056 Å), the diffraction in 2θ range above 0.3 ° was measured. GC plate (1x5 cm) with deposited AgNF was directly mounted into the sample holder of the diffractometer.

***DFT calculations***

All calculations were provided using ORCA 4.0.1.2 software.[58] PBE[59,60] exchange-correlation potential was utilized together with def2-SVP[61,62] basis set. The resolution of the identity[63] approach was applied in order to speed up the calculations, def2/J basis[64] was chosen as the auxiliary basis set for this approach. Solvent (DMF) effects were accounted within CPCM implicit solvation model.[65] Van der Waals interactions were taken into account applying semi-empirical D3[66,67] atom-pairwise dispersion correction with Becke-Johnson damping scheme.[68]

The initial geometries of the studied organic halides' molecules were calculated using Avogadro[69] 1.1.1 software and preliminarily optimized by the means of molecular mechanics with UFF[70] force field, as implemented in OpenBabel[71] 2.3.2 library driven by Avogadro. The resulted UFF-optimized geometries were used as the starting point for DFT optimization of the neutral (charge 0, multiplicity 1) species representing the corresponding non-reduced molecules. Each reduction step was simulated by addition of the electron and re-optimization of the resulted species, the starting point for the optimization of each consequent species was taken from the equilibrium geometry of the previous one. The multiplicity of each consequent species was deduced from the result of the DFT-calculation of the previous one (comparing its α- and β-LUMO energies[72]). Before each DFT geometry optimization, the initial geometry was slightly randomly distorted using a small AWK script (see SI) in order to lower probability of accidental trapping into a saddle point.

View Article Online
DOI: 10.1039/C8NJ03460E



In order to elucidate the stability of the selected species toward possible elimination of Br, the energetic profile of the corresponding C–Br bond elongation was examined by the means of relaxed surface scan (RSS) procedure, as implemented in ORCA, similarly to previously reported methodology.[72] Within each scan, a series of geometry optimizations with constrained C–Br distance was provided for the target species (the other coordinates were not constrained). The C–Br distance was first set to its equilibrium value for the initial scan step and elongated by 0.2 Å on each consequent step (10 steps in total, which corresponds to the total elongation by 2 Å).

## Results and discussion

### *Nanoporous silver foam preparation*

Nanoporous silver foam was prepared by adaptation of the general method for metallic foams formation upon cathodic electrodeposition of metal at high overvoltages or high current densities from aqueous acidic solutions.[43] In our study the foam was formed by reduction of silver from acidic aqueous solution, containing 0.01 M of $AgBF_4$ and 2 M $HBF_4$ at constant current density 3 A/cm$^2$ on GC electrode. This value of current density was chosen as typical value, similarly to reported in literature.[43] It should be noted, that the current density was referred to the geometric area of the GC electrode. 60 s process time was sufficient for deposition of *ca.* 0.5 mg/cm$^2$ of silver deposit. At such conditions hydrogen evolution reaction concurs with metal deposition forming hydrogen bubbles that serve as "soft template" which limits the growth of silver seeds and prevents formation of compact deposit. It should be noted, that only *ca.* 0.25 % of the charge passed through the cell resulted in the silver deposition. Compared to nanoporous silver foam formation in similar system,[32] we simplified the electrolyte composition and used the mixture of $HBF_4$ and $AgBF_4$ instead of $Ag_2SO_4$, KSCN and $NH_4Cl$. In the present study, tetrafluoroborate anion was chosen due to its electrochemical inertness in wide range of cathodic or anodic potentials along with solubility of its salts with $Ag^+$.

Glassy carbon was used as a support for AgNF due to its electrochemical and chemical inertness as well as high overvoltage in reactions of electrochemical reduction of organic halides (at least *vs* smooth silver),[51] which was important for studies of the properties of AgNF in dehalogenation processes.

AgNF was formed on the surface of GC electrode as a matt grey film (Fig. 1), in different experiments with identical conditions the colour of the film varied from dark to light grey. Such deposit was mechanically stable and in the dominating majority of experiments it did not exfoliate spontaneously or upon immersion of the electrode in the solutions in further experiments (*vide infra*), as well as upon stirring the solution. Only rare occasions of the

View Article Online
DOI: 10.1039/C8NJ03460E



exfoliation were observed after a series of experiments, associated with immersion of the electrode in the electrolyte/removing from the electrolyte, as well as agitation of the solution with immersed electrode caused by stirring or argon bubbles. AgNF could be almost completely removed from the GC surface by polishing with filter paper; however, polishing with alumina powder was required for complete removal of silver traces, as shown by CV measurements.

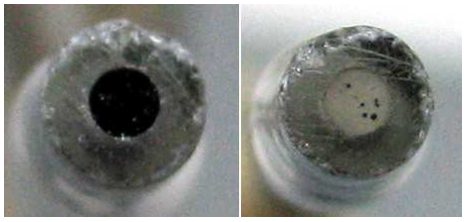

Fig. 1. A photo of the GC disk electrode coated with AgNF (right) and the blank GC electrode (left). The contrast of the images was enhanced in Gimp software.

The process of AgNF electrodeposition was monitored by chronopotentiometry. The initial potential ($E$) of the process was between –3.95 and –3.80 V. In *ca*. 3 seconds $E$ abruptly grew to *ca*. –3.6 V, this change could be caused by formation of metallic silver on GC surface - silver has moderate $H_2$ evolution overpotential[73] while glassy carbon activity in this reaction is negligible.[74] After this initial period $E$ gradually increased reaching *ca*. –3.3 V at the end of the process ($t$ = 60 s). This change could be associated with increase of the electrode surface area in the course of the foam deposition due to increase of the surface roughness which could result in the decrease of effective resistance of the cell (as mentioned, current density was fixed at the value of 3 A/cm$^2$, counting per GC electrode surface, and in order to preserve permanent current value, the absolute value of the potential was decreased by the potentiostat upon decrease of the resistance). All time the potential oscillated in range ΔE *ca.* 100 mV (Fig. 2). Such oscillations could be explained by chaotic changes of the electrochemically accessible electrode surface, associated with the formation and separation of hydrogen bubbles, and could evidence for highly non-equilibrium nature of the process. However, the general trend of the potential change during the process was well-reproducible, as could be concluded from the comparison of E *vs*. *t* curves for formation of several samples of foam in different experiments (Fig. 2).

View Article Online
DOI: 10.1039/C8NJ03460E



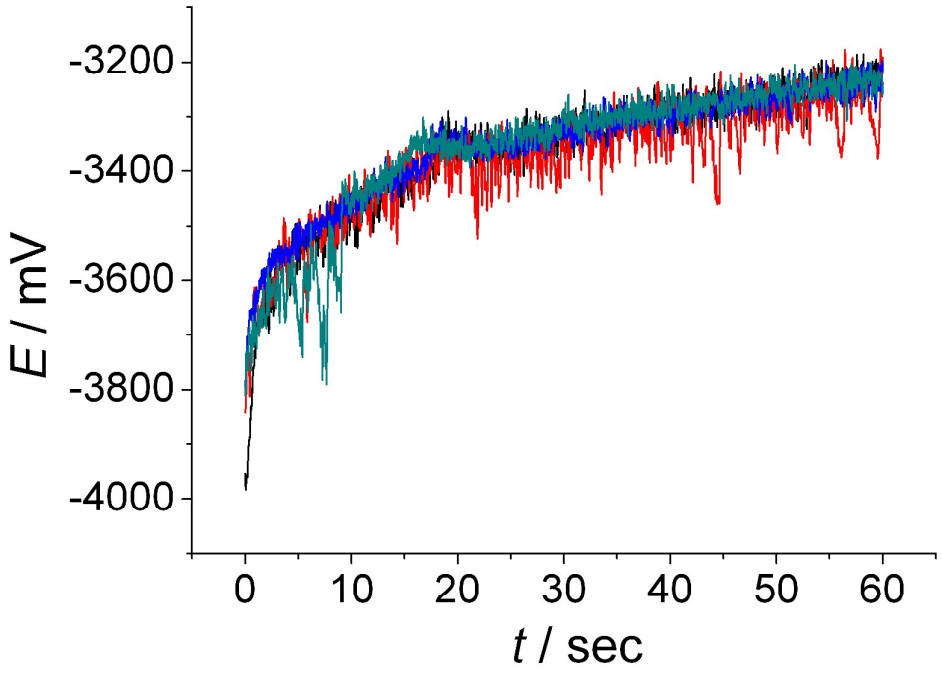


Fig. 2. Chronopotentiograms of four subsequent depositions of the nanoporous silver foams onto the GC disk electrode (different colours denote depositions of different samples).

Since the maximum values of potential and current generated by a potentiostat were limited, at 3 A/cm$^2$ current density we could produce the foam on GC electrode which surface did not exceed 1 cm$^2$. In order to prepare larger GC electrodes coated with AgNF for X-ray diffraction experiment, as well as in order to develop method for potential production-scale applications (such as electrolysis), we performed step-by-step electrodeposition. The whole surface of a large GC electrode was divided into a set of fragments, which were sufficiently small to achieve required high current density (3 A/cm$^2$) if used as independent electrodes. The electrode was covered by paraffin in such way, that only selected fragment was accessible for electrochemical process, the foam was deposited on this fragment, then the paraffin was removed by hot *n*-heptane and the next fragment was covered by AgNF by the same procedure (see Experimental section for details). Such approach allowed preparing AgNF on large GC electrode, ensuring that the whole sample was formed at similar current density. The examination of optical microphoto images of the GC plate covered by AgNF in the stepwise manner showed that the AgNF generally did not change upon consequent application and dissolution of paraffin (Fig. S2). Some scratches (300–600 μm large) on the AgNF appeared, mostly located on the parts where AgNF was formed on the previous step (Fig. S2), but the foam-like structure remained uncollapsed.

***Structure of the AgNF***

View Article Online
DOI: 10.1039/C8NJ03460E



The X-ray diffraction pattern of AgNF/GC (Fig. 3) was consistent with the presence of metallic silver. No reflections, corresponding to other crystalline phases such as $Ag_2O$ were found. However, there was the intense halo originated from the GC support, which could obscure reflections of low intensity (if any). It can not be excluded that AgNF consists of several phases, but among crystalline phases (if any additional phases are present) Ag metal is dominating.

The full width at half maximum of the most intense reflection, originating form the (111) system of planes, was 0.239 °, which corresponded to *ca.* 40 nm size of coherent scattering region estimated from the Scherrer equation assuming shape factor equal to 0.9 (spherical crystallites).[75]

It can be noted that no peaks were found in low-angle region ($2\theta < 3$ °) of the powder diffraction pattern (Fig. S3). At the same time, ordered mesoporous materials such as non-crystalline molecular sieves MCM-41 or FSM-16 can have reflections on powder XRD patterns in low angle region above $2\theta = 0.3$ °.[76] We can conclude that AgNF does not possess regular mesoporous structure with interplanar distance $d < 30$ nm.

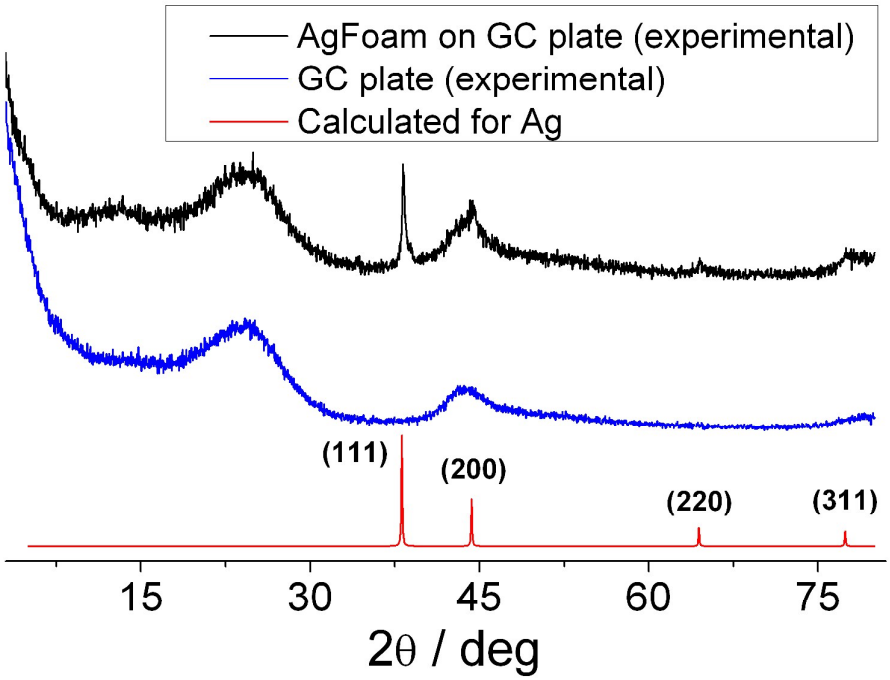


Fig. 3. Experimental XRD pattern of the AgNF/GC and clean GC plate, as well as the pattern calculated from single-crystal X-ray data for silver [77] (obtained via Crystallography Open Database [78], COD ID 9008459) .

Investigation of the surface of the silver deposit via optical microscopy (Fig. 4) confirmed its foam-like structure with irregular cells *ca.* 20 μm in diameter with walls of *ca.* 7 μm in thickness. The walls were not smooth; the granulae could be distinguished on their surfaces (the sizes of the granulae were about a few micrometers).

View Article Online
DOI: 10.1039/C8NJ03460E



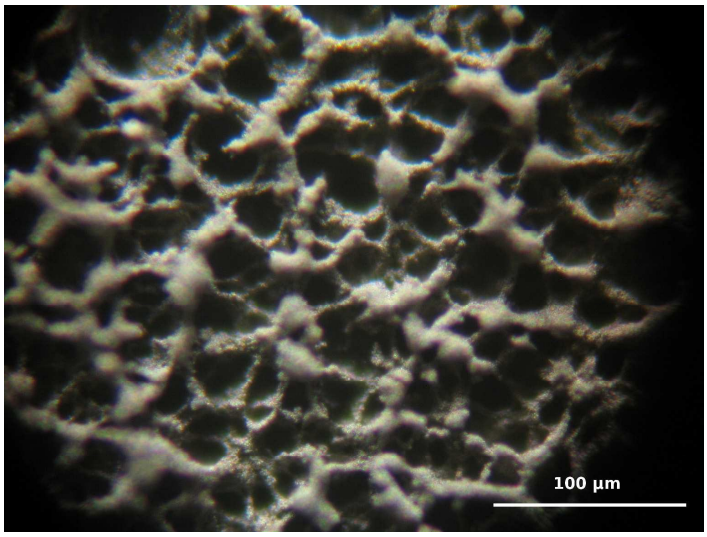


Fig. 4. Silver nanofoam under optical microscope.

The results of scanning electron microscopy (Fig. 5) revealed that the walls of the craters possessed dendrite-like structure. The thickness of the silver filaments was in range 100–300 nm.

The above mentioned granulae distinguished on surfaces of the walls on optical microscopy images were not observed on the SEM images. These granulae could be attributed to bunches of silver filaments that could not be resolved into separate filaments by optical microscopy due to their size lower than diffraction limit for visible light.

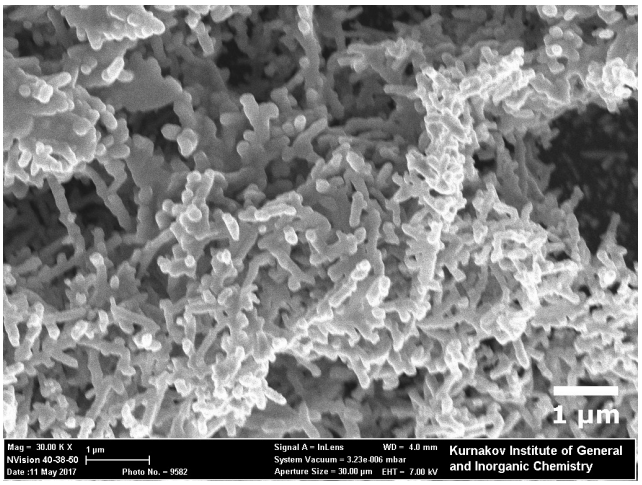


Fig. 5. SEM image of AgNF.

In order to provide more detailed investigation of the structure of the smallest elements of AgNF structure we destructed an AgNF sample by ultrasonication in isopropyl alcohol (considered as inert solvent) and studied the resulting particles by transmission electron microscopy. Aggregated filaments were found on TEM images (Fig. 6), their thickness was 70–150 nm (ca. 100 nm in average). The thickness of the filaments determined by TEM was lower

View Article Online
DOI: 10.1039/C8NJ03460E



than determined by SEM (*vide supra*), that could be caused by their partial splitting upon ultrasonication. However, the thickness determined by SEM could be overestimated, as the filaments on the SEM image were oriented mostly not parallel to the photograph plane, and, thus, thicker parts of the filaments could hide the thinner ones, resulting in bias of the mean value estimation. Additionally, scarce quantities of smaller nanoparticles (5–30 nm) were observed on the surface or in the vicinity of the filaments. These particles could originate from the electrodeposition process (being integral parts of the filaments) or from ultrasonic destruction of larger aggregates (being attracted to the surface of the filaments by capillary forces during drying of the sample prepared for TEM). Electron diffraction pattern (Fig. 7) could be explained as originating from polycrystalline silver samples, though only the first ring corresponding to the distances between the planes with (111) Miller indices could be distinguished (Fig. S4).

No distinct facets of the filaments were observed on the TEM images which suggested that the filaments were aggregates of crystallites rather than isolated single crystals. Additionally, darker spots and lines could be distinguished within some (lighter) filaments on these images which could be attributed to boundaries between crystalline grains and/or to defects of the crystal structure.

There was a halo with thickness up to a dozen of nanometers at the edges of the silver filaments. While the exact origin of the halo was unclear for us, it could be suggested that it originated from products of superficial oxidation of silver (silver oxide and/or silver fluoride). This suggestion regarding the presence of oxide of fluoride layer on Ag surface is consistent with the results of cyclic voltammetry measurements, *vide infra*.

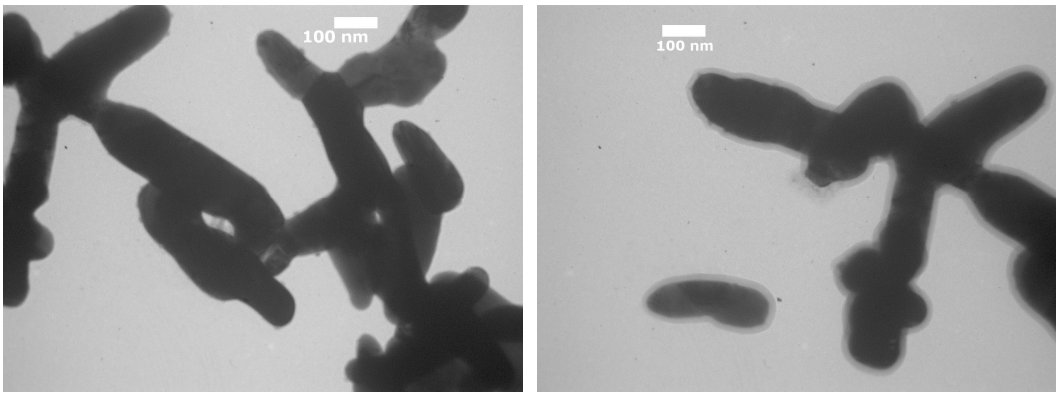


Fig. 6. TEM images of the destructed AgNF.

View Article Online
DOI: 10.1039/C8NJ03460E



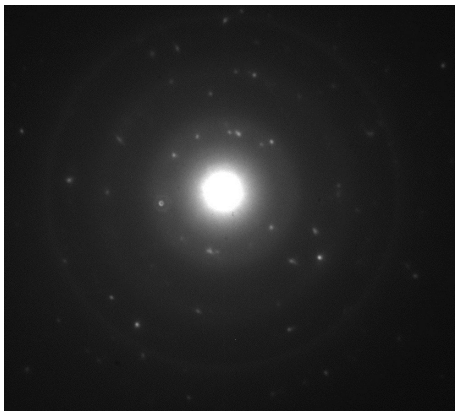

Fig. 7. Electron diffraction image of the sample of AgNF prepared for TEM.

Thus, generally the structure of AgNF can be described as small silver crystals of size *ca*. 40 nm (coherent scattering region size estimated by XRD measurement), which are assembled in "nanorods" of size in range *ca*. 70–300 nm (estimated from TEM and SEM experiment); in turn, such nanorods are arranged in foam-like structure with cavities of size *ca*. 20 μm and walls of thickness *ca.* 7 μm (found by optical microscopy). Such arrangement can be considered as a system with structural hierarchy.[79]

Silver nanofoams with similar structure synthesized by cathodic electrodeposition (in galvanostatic mode at 1 A/cm$^2$ current density) of silver from electrolyte containing $Ag_2SO_4$ (0.01 M), KSCN (1.5 M) and $NH_4Cl$ (0–2 M) were reported previously.[32] Bubble-like cavities reported in ref.[32] were typically larger (20–45 μm) than in current work; other dimensions were not reported by authors in text, but as far as it could be deduced from the reported figures, they were consistent with the dimensions reported herein (except coherent scattering region size which can not be compared because of lack of XRD data in ref.[32]). It should be noted that the electrodeposition occurred at roughly the same potentials (–3..–4 V *vs* Ag/AgCl) and threefold lower current density (–1 A/cm$^2$ in ref.[32] and –3 A/cm$^2$ in our work), which could indicate that in our work the electrodeposition underwent easier than in ref.[32] This observation could be explained by different electrolyte composition. In particular, in order to synthesize metal nanofoam by cathodic electrodeposition, one should ensure simultaneous deposition of silver and hydrogen evolution. For this aim, the electrolyte should contain the ions which are the sources of elementary silver and hydrogen in appropriate concentrations. In our work, hydrated $Ag^+$ cations (more specifically, their cationic aqua-complexes $[Ag(H_2O)_n]^+$) from $AgBF_4$ were sources of silver, and hydrated $H^+$ ions from $HBF_4$ were sources of hydrogen. In ref.[32], allegedly anionic thiocyanate complexes $[Ag(SCN)_x]^{1-x}$ were sources of silver and $NH_4^+$ cations were sources of hydrogen; the latter was additionally proven by failure to obtain nanofoam in the absence of $NH_4Cl$. Reduction $[Ag(H_2O)_n]^+$ cations in our case occurs more readily compared to

View Article Online
DOI: 10.1039/C8NJ03460E



$[Ag(SCN)_x]^{1-x}$, and hydrated protons in our case are more active than $NH_4^+$ cations at comparable concentrations. Thus, though the relative activity of both required components for the cathodic reactions was acceptable herein and in ref.[32], their absolute activity was higher in our work. As a consequence, similar result could be obtained more easily by our approach than by approach reported in ref.[32]

***Electrochemical properties of the AgNF/GC***

Cyclic voltammograms of neat electrolyte solution (DMF) on AgNF/GC working electrode (an example of such CV was presented on Fig. S5) indicated stability ("electrochemical window") of the foam in potential range from *ca.* −2500 mV (limited allegedly by electrolyte decay on the cathode) to *ca.* −100 mV (limited by silver anodic dissolution). Wide poorly reproducible peaks with current up to a dozen of microamperes (2 mm AgNF/GC disk) were observed on the cathodic branch of the CV in range *ca.* −500..−1250 mV that could be attributed to reduction of superficial oxide or fluoride layer of AgNF. Their poor reproducibility could be explained by significant dependence of the superficial layer state on the history of the sample. These peaks will not be discussed in description of CVs of halides reduction.

Electrochemically accessible specific surface area of AgNF was estimated by comparison of pseudo-capacitance of AgNF/GC and smooth silver electrodes by the means of cyclic voltammetry[57] (see Experimental section for details). It was found that the specific surface of AgNF/GC samples was in average *ca.* 8 times higher than the specific surface of the smooth silver electrode. Adopting roughness factor 1.5 for smooth silver[57], the area of the AgNF could be estimated as 2.4 $m^2/g$, which was 12 times higher than the geometrical area (taking into account the above mentioned estimation of the nanofoam mass). This specific surface area was in good agreement with the specific surface calculated for ideal endless silver nanorods with diameter equal to 150 nm (2.54 $m^2/g$).

**Performance of AgNF in electrochemical reduction of organic halides**

The performance of AgNF/GC, smooth silver and GC working electrodes in the electrochemical reduction of a series of organic halides was compared by analysis of cyclic voltammograms of their solutions in anhydrous DMF on the corresponding working electrode.

***Aryl bromides - bromobenzene, 1-bromo-4-fluorobenzene and 1-methoxy-4-bromo-2,6-dimethylbenzene.***

Cyclic voltammograms of 5.5 mM bromobenzene in DMF (with 0.1 M $Bu_4NBF_4$ as supporting electrolyte) on different working electrodes (GC, smooth silver and AgNF/GC) are

View Article Online
DOI: 10.1039/C8NJ03460E



presented on Fig. 8 a)). There was one irreversible reduction peak on each voltammogram that could be attributed to reduction of bromobenzene (yielding benzene according to literature data[80]). The potential $E_{pc}$ of the cathodic peak (referred as P1A, see Fig. 8 a)) on AgNF/GC electrode (−1593 mV) was 344 mV less negative than on the smooth silver, which, in turn, was 741 mV less negative than on glassy carbon electrode. Additionally, a shoulder (referred as P1B) at the potential −1799 mV could be distinguished on the CV on AgNF/GC. The possible origin of such shoulder will be discussed below. The currents $i_{pc}$ at the $E_{pc}$ values on the cathodic branch of the CV were comparable by magnitude (40–80 μA).

Similar situation took place in the case of substituted bromobenzenes: 1-bromo-4-fluorobenzene and 1-methoxy-4-bromo-2,6-dimethylbenzene (Fig. 8 b), c)). The potentials of their reduction peaks (Table 1) were shifted compared to those for bromobenzene, but their order was preserved. Contrary to bromobenzene and 1-bromo-4-fluorobenzene, only one peak was found on the CV of 1-methoxy-4-bromo-2,6-dimethylbenzene on AgNF/GC, no additional peaks or shoulders were present. Again, $i_{pc}$ values on smooth silver and GC were comparable with the correspondent $i_{pc}$ values on AgNF/GC.

The observed difference in the potentials of the peaks could evidence for electrocatalytic activity of the nanoporous silver foam in reduction of the studied aryl bromides that was higher than the activity of the smooth silver. Different peak potentials on the smooth Ag and AgNF/GC electrodes could be explained by existing of some active sites (probably, a few kinds of such sites which could be deduced from presence of shoulders on some peaks as discussed below) on the surface of the foam that facilitate the reduction of the aryl bromides. Similarly, formation of active centres able to promote $CO_2$ reduction was previously reported for nanoporous silver obtained by dealloying of AgAl alloy[34]. The charges consumed on the cathodic branch of the CVs of the studied aryl bromides on AgNF/GC were comparable with the respective charges for smooth silver despite 8-fold difference in electrochemically accessible surface area (*vide supra*) of these electrodes. Absence of noticeable consumed charge difference can be explained by limitations of the reagents diffusion from the bulk solution into the inter-filament space of the foam in the frames of cyclic voltammetry experiments rather than insufficient quantities of the active sites. Allegedly, the molecules of the aryl bromides on electrode were reduced only on such active sites, and the rest of the surface was inactive due to exhausting of the substrate in the vicinity of the electrode. Presence of two peaks (or a peak with an additional shoulder) on the cathodic branches of the CVs of some compounds could be explained by the existence of two or more types of the active centres.

Assignment of the peaks on CVs of bromobenzene, 1-bromo-4-fluorobenzene and 1-methoxy-4-bromo-2,6-dimethylbenzene seems to be unambiguous, because elimination of $Br^-$ is

View Article Online
DOI: 10.1039/C8NJ03460E



the preferred process.[80] This is not the case for other aromatic halides, studied in this work, which will be discussed below. For peak assignment DFT calculations of all studied halides reduction were performed (see Experimental section). The results of DFT investigation of bromobenzene, 1-bromo-4-fluorobenzene and 1-methoxy-4-bromo-2,6-dimethylbenzene reduction suggested that addition of one electron to a solvated aryl bromide molecule (yielding the corresponding anion-radical) led to barrierless elongation of C–Br bond by *ca.* 0.9 Å accompanied by decrease of C–Br Mayer[81] bond order to *ca.* 0.3 (Table SI_DFT). Further increase of C–Br distance by RSS procedure led to energy oscillations within 10 kJ/mol (Fig. S6) which could be easily overcome by energies of thermal movement. The described behaviour corresponded to actual cleavage of C–Br bond in result of one-electron reduction. Though simple addition of electron referred rather to adiabatic excitation of the molecules rather than followed the genuine pathway of the reduction process, the barrierless elimination of bromide evidenced towards instability of bromobenzene anion-radical and therefore towards concerted mechanism of C–Br bond cleavage rather than towards stepwise one.[44]

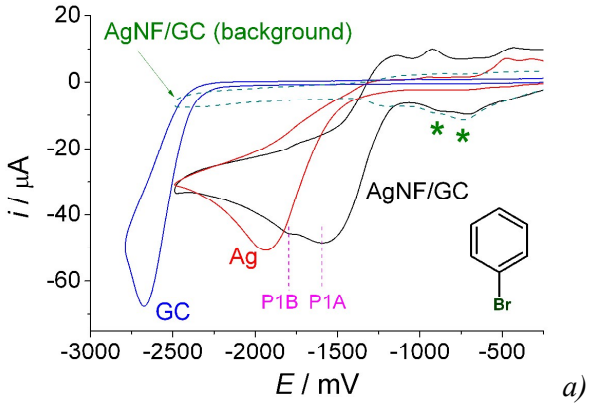


*a)*

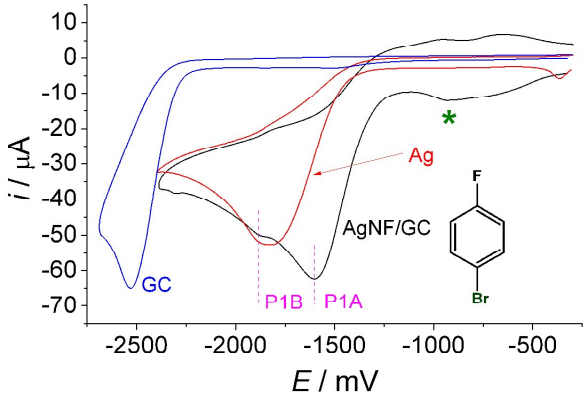


*b)*

View Article Online
DOI: 10.1039/C8NJ03460E



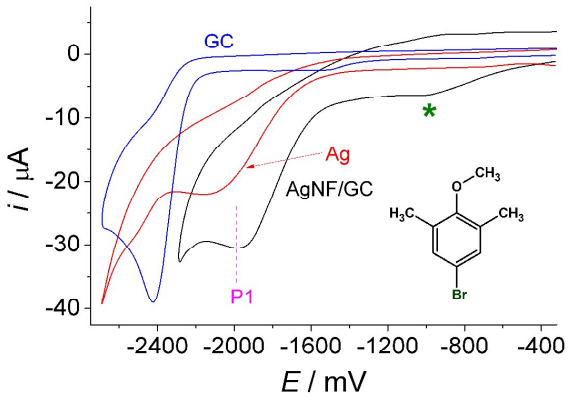


c)

Fig. 8. Cyclic voltammograms of the solutions of a) bromobenzene (5.5 mM), b) 1-bromo-4-fluorobenzene (5.3 mM) and c) 1-methoxy-4-bromo-2,6-dimethylbenzene (2.6 mM) on AgNF/GC, smooth silver (Ag) and GC disk electrodes (d = 2 mm for all electrodes, which corresponded to geometric surface area 3.14 $mm^2$) as well as cyclic voltammogram of neat background electrolyte on AgNF/GC. Medium: 0.1 M $Bu_4NBF_4$ in DMF, scan rate – 100 mV/s, potentials *vs.* Ag/AgCl reference electrode. The peaks attributed to silver oxide or fluoride reduction are marked by asterisk.

Table 1. Reduction peak potentials $E_{pc}$ of the studied substances (italic font means shoulder instead of peak).

| Substance | | $-E_{pc}$, mV *vs* Ag/AgCl | | | |
|---|---|---|---|---|---|
| | | AgNF/GC | | Smooth Ag | GC |
| | | A | B | | |
| Bromobenzene | | 1593 | *1799* | 1937 | 2678 |
| 1-bromo-4-fluorobenzene | | 1603 | *1883* | 1830 | 2531 |
| 1-methoxy-4-bromo-2,6-dimethylbenzene | | 1987 | – | 2164 | 2424 |
| 1-bromo-1-chloro-2,2,2-trifluoroethane | | 1232 | 1453 | 1465 | 1686 |
| dibromodifluoromethane | | *998* | 1083 | 1067 | 1425 |
| 1-(4-bromo-3-fluorophenyl)ethanone | P1 | 1333 | *1632* | 1420 | 1592 |
| | P2 | 1885 | – | 1888 | 1885 |
| 1-bromo-4-fluoro-2-nitrobenzene | P1 | 1067 | – | 1063 | 1029 |
| | P2 | 1972 | – | 2079 | 2065 |
| 3-bromo-4-(trifluoromethyl)benzonitrile | P1 | 1175 | 1397 | 1449 | 1570 |
| | P2 | 1990 | – | 2017 | 2015 |
| | P3 | *2373* | – | 2367 | 2366 |

*Comparison of voltammograms of bromobenzene on different AgNF/GC samples.* In order to evaluate if the described procedure of AgNF/GC formation was reproducible, we compared cyclic voltammograms (Fig. 9) of bromobenzene solutions on 4 independently formed

View Article Online
DOI: 10.1039/C8NJ03460E



AgNF/GC samples. It was found that on the first CV scans the $E_{pc}$(P1A) (P1A cathodic peak potential) corresponding to electrochemical reduction of bromobenzene changed in range −1670..−1520 mV, and $i_{pc}$(P1A) (the current at $E_{pc}$(P1A) on the cathodic branch of the CV) varied in range −46..−62 mA. Such scatter of the values could be caused by highly non-equilibrium conditions of the nanofoam formation. Contrary to that, the reproducibility of $E_{pc}$(P1B) and $i_{pc}$(P1B) was significantly higher.

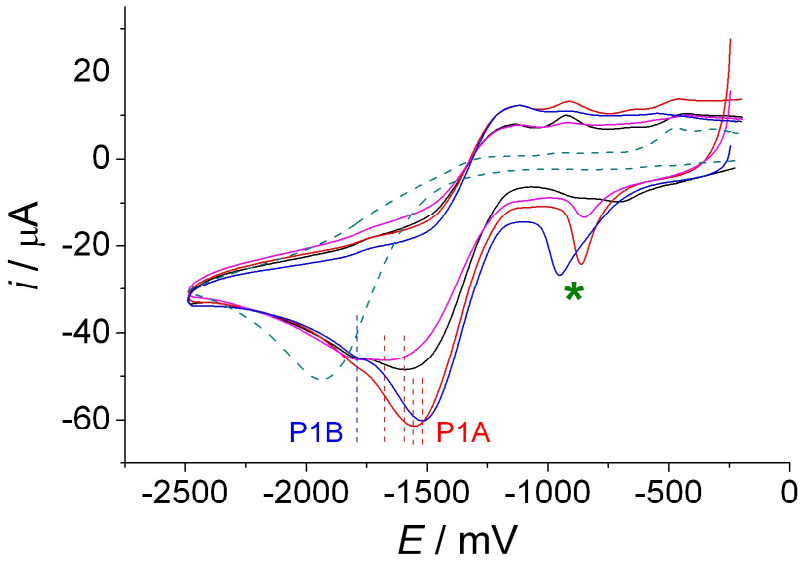


Fig. 9. Cyclic voltammograms (1st scans only) of the solution of bromobenzene (5.5 mM) on 4 different AgNF/GC samples (d = 2 mm). Solid lines with different colours indicate different independently prepared samples of the nanofoam, dashed line corresponds to CV of the same solution on smooth silver electrode. Red vertical dashed lines mark position of P1A peak of bromobenzene reduction, blue one – P1B position. Medium: 0.1 M $Bu_4NBF_4$ in DMF, scan rate – 100 mV/s, potentials *vs.* Ag/AgCl reference electrode. The peaks attributed to silver oxide or fluoride reduction are marked by asterisk.

*Reproducibility of voltammograms on the same AgNF/GC sample.* A series of cyclic voltammograms of bromobenzene solution on a single sample of AgNF/GC was recorded (Fig. 10), after each complete scan the scanning was stopped and the working solution was thoroughly stirred by magnetic stirrer. The voltammograms of the consequent scans revealed relatively high reproducibility, no systematic potential shift or current change of the cathodic peak was observed ($i_{pc}$(P1A) were slightly lesser by magnitude on the first two scans). A few other samples of AgNF/GC manifested the same behaviour (Fig. S7). Thus, it could be concluded that AgNF/GC didn't undergo degradation under such experimental conditions.

View Article Online
DOI: 10.1039/C8NJ03460E



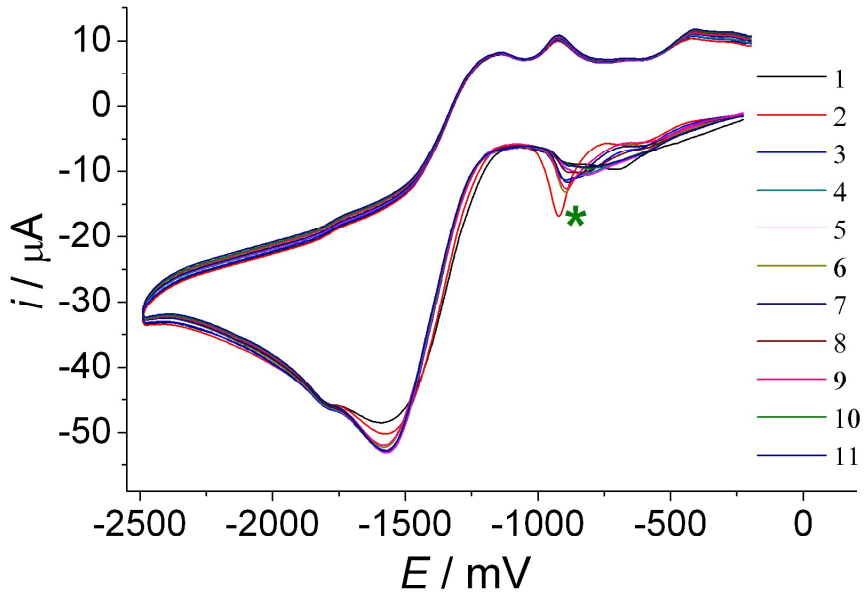


Fig. 10. Cyclic voltammograms of the solutions of bromobenzene (5.5 mM) on AgNF/GC (d = 2 mm). 11 consequent scans were presented, after each one the scanning was stopped and the working solution was thoroughly stirred. Medium: 0.1 M $Bu_4NBF_4$ in DMF, scan rate – 100 mV/s, potentials *vs.* Ag/AgCl reference electrode. The peaks attributed to silver oxide or fluoride reduction are marked by asterisk.

A similar series of CVs was recorded for 1-bromo-4-fluorobenzene solution on AgNF/GC, but the working solution was stirred only before some selected scans (Fig. 11). Absence of stirring before the scan led to noticeable decrease (*ca.* 10 μA) of the $i_{pc}$ values that could be caused by exhausting of 1-bromo-4-fluorobenzene in the vicinity of the electrode, and to some anodic $E_{pc}$(P1A) shift. After stirring, the $i_{pc}$(P1A) values almost restored, accompanied by partial restoration of the initial $E_{pc}$(P1A) value, while the restoration of the $i_{pc}$(P1B) value was noticeably poorer. However, as P1B was a shoulder or a tiny peak against significantly larger P1A, it was not clear, if such difference was caused by real decrease of faradaic current of the electrochemical process associated with P1B, or the observed difference could be explained by differences in $E_{pc}$, $i_{pc}$ and width of P1A. In general, the electrocatalytic activity of AgNF/GC in reduction of 1-bromo-4-fluorobenzene was preserved upon scanning in this regime.

View Article Online
DOI: 10.1039/C8NJ03460E



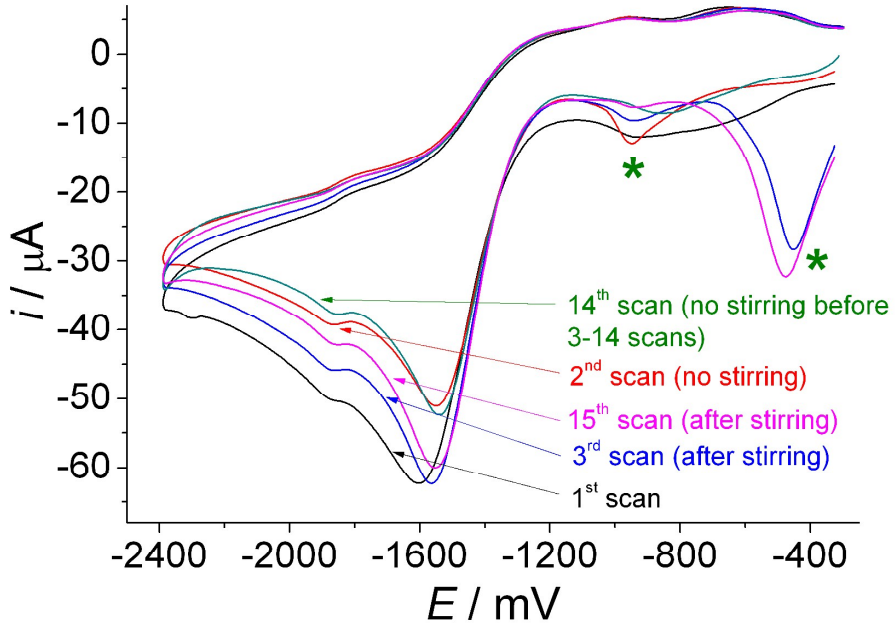


Fig. 11. Cyclic voltammograms of the solutions of 1-bromo-4-fluorobenzene (5.3 mM) on AgNF/GC (d = 2 mm). 15 consequent scans were performed, the electrolyte was stirred before the 3rd and 15th one. Medium: 0.1 M $Bu_4NBF_4$ in DMF, scan rate – 100 mV/s, potentials *vs.* Ag/AgCl reference electrode. The peaks attributed to silver oxide or fluoride reduction are marked by asterisk.

***Aryl bromides with additional functional group that can undergo electrochemical reduction.***

As shown, the potentials of the debromination processes involving aryl bromides were shifted to positive values upon use of AgNF/GC as electrode. In order to reveal if similar potential shift occurred in the case of processes, based on reduction of other functional groups, we measured cyclic voltammograms of substituted bromobenzenes with –CN, $–NO_2$ and $–COCH_3$ groups (Fig. 12). Expectedly, a few peaks were found on the cathodic branches of each voltammogram (some of them with counter-peaks) which could be attributed to reduction of different functional groups.

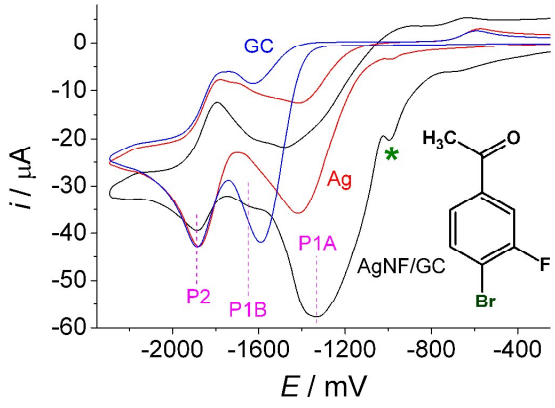


*a)*

View Article Online
DOI: 10.1039/C8NJ03460E



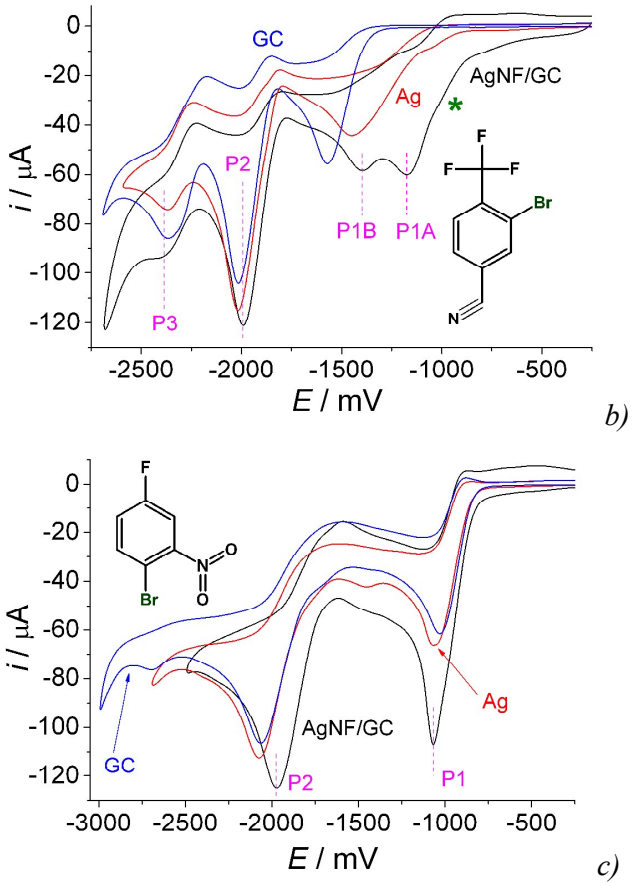


Fig. 12. Cyclic voltammograms of the solutions (5 mM) of substituted bromobenzenes (bearing additional functional group that could undergo electrochemical reduction) on AgNF/GC, smooth silver and glassy carbon disk electrodes (d = 2 mm, for all electrodes, which corresponded to geometric surface area 3.14 $mm^2$). Medium: 0.1 M $Bu_4NBF_4$ in DMF, scan rate – 100 mV/s, potentials *vs.* Ag/AgCl reference electrode. The peaks attributed to silver oxide or fluoride reduction are marked by asterisk.

Three peaks (denoted as P1A, P1B (shoulder) and P2) were found on the CV of 1-(4-bromo-3-fluorophenyl)ethanone solution (Fig. 12 a)) on AgNF/GC working electrode. P2 peak had a counter-peak on the anodic branch of the CV, while P1A didn't (for P1B it was difficult to make a reliable conclusion). Two peaks were also observed on the CVs of the same compound on smooth silver and GC electrodes: one peak on GC and one peak on smooth silver had virtually the same potential as P2, while the potentials of the other peaks was not close to each other and to P1A or P1B ($E_{pc}$ increased in the row AgNF/GC(P1B) < GC < smooth silver < AgNF/GC(P1A)).

Similarly, four peaks were found on the CV of 3-bromo-4-(trifluoromethyl)benzonitrile on AgNF/GC *vs.* three peaks on smooth silver and GC (Fig. 12 b)). There were two peaks on smooth silver and two peaks on GC with potential close to P2 and P3 peaks (all of them with counter-peaks on the anodic branches of the CVs). The other peak on smooth silver was close to

View Article Online
DOI: 10.1039/C8NJ03460E



P1B, while the rest of the peaks had potentials not close to each other and to above mentioned peaks (all of them without counter-peaks).

Two peaks were found on the CV of 1-bromo-4-fluoro-2-nitrobenzene (Fig. 12 c)) on AgNF/GC, smooth silver and GC. The potentials of the peaks did not differ significantly on different electrode materials (P2 had potential slightly lesser by magnitude than the corresponding peaks on smooth silver and GC).

For assignment of peaks on CVs of 1-(4-bromo-3-fluorophenyl)ethanone, 3-bromo-4-(trifluoromethyl)benzonitrile and 1-bromo-4-fluoro-2-nitrobenzene reduction, DFT analysis of their reduced forms was carried out, as described above. In contrast to bromobenzene or substituted analogues with F, $CH_3$ and $OCH_3$ groups, one-electron reduction of the compounds with $COCH_3$, CN and $NO_2$ functions did not lead to C–Br bond cleavage. In the case of $COCH_3$, CN-substituted bromobenzenes significant elongation of C–Br bond and reduction of its order occurred only upon addition of the second electron, while for nitro-compound even two-electron reduction did not lead to dehalogenation. Thus, in contrast to bromobenzene, dehalogenation of $COCH_3$ and CN-substituted analogues occurs in two-step pathway (stepwise). It was previously reported [82,83] that electrocatalytic effect of smooth silver cathodes in reductive dehalogenation (compared to non-catalytic GC ones) significantly depended on the reduction mechanism, with one-step (concerted) cleavage of C–Br bond associated with notably higher potential shifts compared to stepwise cleavage. Our results reported herein supported that conclusions regarding smooth silver. However, despite there were signs of similar effect when comparing reduction on AgNF/GC and smooth Ag, we consider that the present results were not statistically sufficient to reliably confirm it. In the case of 1-bromo-4-fluoro-2-nitrobenzene the peak P1 almost did not shift at AgNF/GC compared to Ag or GC, instead positive shift of P2 peak was found. These observations were completely consistent with the results of DFT calculations, which implied that the first process could be assigned to reduction of $NO_2$ group, while the second could be associated with C–Br bond cleavage in this case.

***Alkyl bromides - halothane and P1B for $CF_2Br_2$.***

CVs of two alkyl bromides – halothane (1-bromo-1-chloro-2,2,2-trifluoroethane) and $CF_2Br_2$ – were studied on AgNF/GC, smooth Ag and GC electrodes. Similarly to bromobenzene, one distinct peak (P1A for halothane and P1B for $CF_2Br_2$) and one tiny peak or shoulder (P1B for halothane and P1A for $CF_2Br_2$) were found on the CVs of halothane and $CF_2Br_2$ on AgNF/GC electrode, while only one peak (Fig. 13) was found on each CVs of the same compounds on smooth silver and GC electrodes. The potentials of the peaks on different electrodes increased in a row GC < smooth Ag ≈ AgNF/GC(P1B) < AgNF/GC(P1A) for

View Article Online
DOI: 10.1039/C8NJ03460E



halothane and GC < AgNF/GC(P1B) ≈ smooth Ag < AgNF/GC(P1A) for $CF_2Br_2$. Similarly to bromobenzene, no significant differences in the CV curve were observed within a series of scans of halothane solution on a single AgNF/GC sample if the solution was stirred before each scan (Fig. S8). Contrary to that, continuous cycling without stirring led to significant irreversible cathodic shift (Fig. 14 a)) of P1A peak (P1B peak could not be distinguished under such conditions). In the case of $CF_2Br_2$ (Fig. 14 b)), cycling in the same regime led to significant reversible decrease of $i_{pc}$(P1A) (the values were almost restored on the next scan after stirring) and had almost no impact on P1B. Similarly to experiments on aryl halides, these observations could be explained by existence of a few types of active centres on the surface of the silver nanofoam that could facilitate the reduction of alkyl halides superior to the surface of smooth silver. These active centres allegedly deteriorated in the course of halothane reduction (contrary to 1-bromo-4-fluorobenzene and $CF_2Br_2$), which could be explained by dissolution of nanoscaled silver at presence of $CF_2$=CHCl (one of possible halothane reduction products[48,49] allegedly able to form π-complexes with silver).

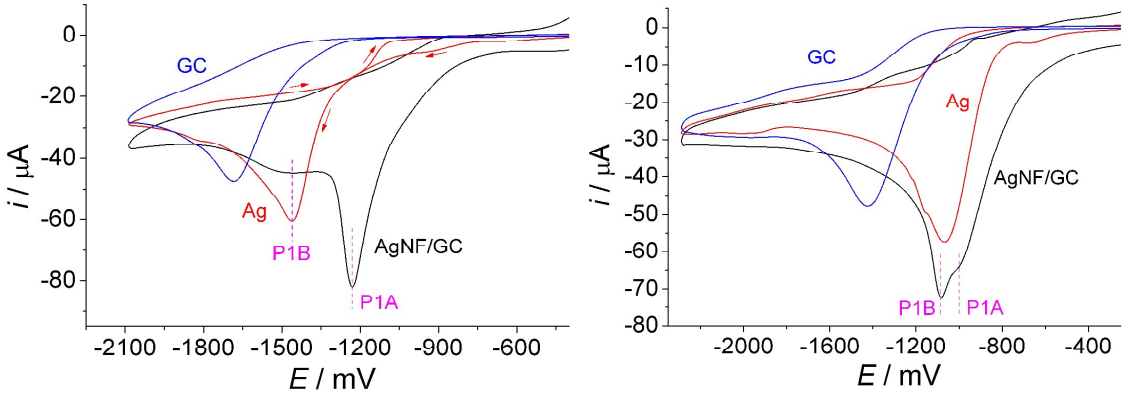


Fig. 13. Cyclic voltammograms of the solutions of halothane (5.5 mM) and $CF_2Br_2$ (3.9 mM)on AgNF/GC, smooth silver and glassy carbon disk electrodes (d = 2 mm). Medium: 0.1 M $Bu_4NBF_4$ in DMF, scan rate – 100 mV/s, potentials *vs.* Ag/AgCl reference electrode.

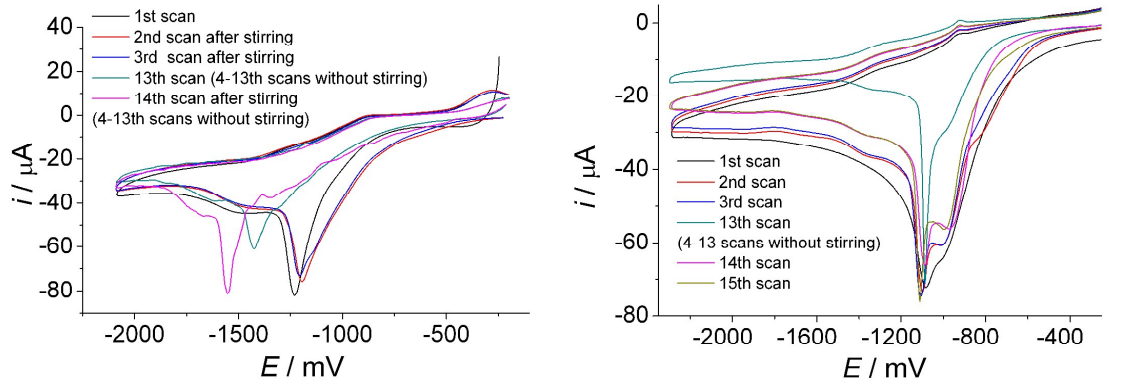

View Article Online
DOI: 10.1039/C8NJ03460E



Fig. 14 Cyclic voltammograms of the solution of halogenalkanes on AgNF/GC (d = 2 mm): a) halothane (5.5 mM), b) $CF_2Br_2$ (3.9 mM). 14—15 consequent scans are presented, the scanning was stopped and the working solution was thoroughly stirred after 1st, 2nd, 3rd and 13th scan. Medium: 0.1 M $Bu_4NBF_4$ in DMF, scan rate – 100 mV/s, potentials *vs.* Ag/AgCl reference electrode.

**Electrolysis of 1-bromo-4-fluorobenzene and halothane**

Solutions of 1-bromo-4-fluorobenzene and halothane (100 μL in 5 mL of the electrolyte) were subjected to electrolysis on AgNF/GC cathode (a GC plate with 30 $mm^2$ of the surface covered by AgNF) in three-electrode undivided cell with Mg sacrificial anode and the reference electrode. The electrolysis was carried out in potentiostatic mode at the potential of the cathodic peak on the corresponding voltammogram (–1603 mV for 1-bromo-4-fluorobenzene and –1232 mV for halothane, peaks P1A on Figs. 8 (b) and 13, respectively). The value of the current was *ca.* 0.6–1 mA (typically, slightly decreasing by absolute value in the course of the process) throughout the entire 1-bromo-4-fluorobenzene electrolysis (Fig. 15 a)). Fluorobenzene (*ca.* 5–6%) was found as the only product after the electrolysis by $^{19}$F-NMR (Fig. S9) investigation of the reaction mixture (δ = –113.1 ppm *vs* $CFCl_3$) which corresponded to faradaic efficiency *ca.* 60 %. Currents in a control experiment in which a neat GC plate was used as the cathode were significantly lower by magnitude (less than 0.2 mA, Fig. 15 a)), no signs of fluorobenzene or other products were found in the reaction mixture of the control experiment after the electrolysis on GC.

For comparison with smooth silver, silver wire electrode was chosen in such way that its area was close to the electrochemically accessible area of AgNF/GC (estimated from pseudo-capacitance measurements, *vide supra*); this value was *ca*. 12 times higher than the geometric value of the AgNF/GC sample. Thus, smooth silver wire of 76 mm length and 1 mm in diameter was used as cathode, its surface corresponds to the electrochemically accessible S = 30 $mm^2$ of AgNF and dozen times exceeds the geometrical area of AgNF sample. The current values in this control experiment were up to 1.5-1.6 times higher than the currents found for AgNF/GC. Higher current values for smooth Ag compared to the value, expected for AgNF/GC assuming that its whole surface would be active in electrolysis, can be explained by hindrances of the external diffusion of substrate in the latter case due to significantly lower geometric area of AgNF/GC compared to smooth Ag. Fluorobenzene was found as the only product in this experiment as well, with ca. 6.5 % yield and ca. 55 % faradaic efficiency which was comparable to values found for AgNF/GC.

Notable increase of current (by absolute value) was found both for AgNF/GC and smooth silver in the initial period of the electrolysis (up to 30 minutes for AgNF/GC and up to 60 minutes for the smooth silver). This effect could be explained by electrochemical reduction of

View Article Online
DOI: 10.1039/C8NJ03460E



superficial silver oxide at the beginning of electrolysis that led to increase of the surface area of metallic silver facilitating the reduction of 1-bromo-4-fluorobenzene.

Contrary to 1-bromo-4-fluorobenzene, a rapid current decay was observed in the course of halothane electrolysis on AgNF/GC (Fig. 15 b)). No signs of electrolysis products were found in the reaction mixture after the electrolysis, as well as AgNF cover was found to be "washed out" from the GC support. These observations were consistent with degradation of AgNF/GC electrocatalytic performance in halothane reduction, similarly to the effect, observed with cyclic voltammetry under continuous cycling without stirring (*vide supra*).

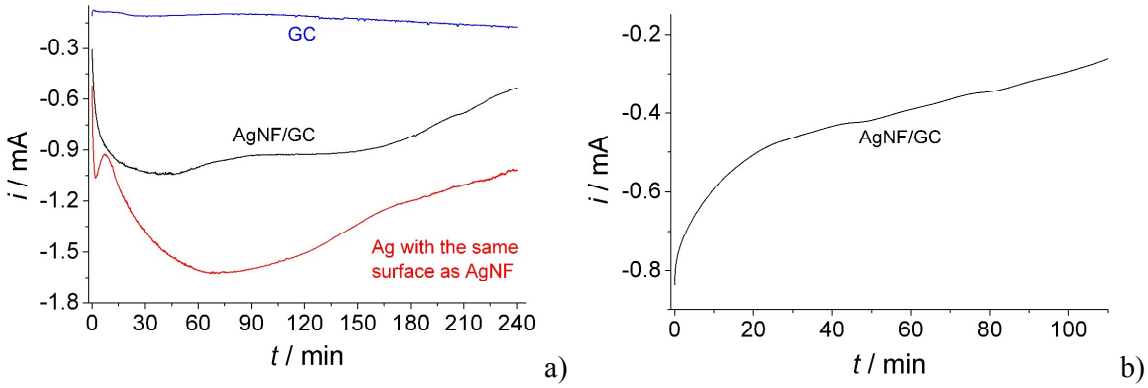


Fig. 15. Chronoamperograms recorded in the course of 1-bromo-4-fluorobenzene (the surface area of silver electrode was taken the same as the surface of AgNF as estimated from the pseudocapacitance measurements, *vide supra*) (a) and halothane (b) electrolysis.

**Conclusions**

In this study it was shown that nanostructured Ag coating on the surface of GC electrode could be created by cathodic deposition of silver from 0.01 M of $AgBF_4$ solution in 2 M $HBF_4$ at 3 A/cm$^2$ constant current density. This approach led to formation of nanoporous Ag foam (AgNF/GC) with could be considered as a system with structural hierarchy: *ca*. 40 nm silver crystals are assembled in *ca*. 70–300 nm “nanorods” which are arranged in foam-like structure with *ca*. 20 μm cavities and *ca.* 7 μm walls. From pseudo-capacitance measurements the area of the AgNF was 12 times higher than the value, expected from the geometrical size of the sample. From TEM results and CVA studies of AgNF/GC it can be concluded, that silver is covered by thin layer of oxide or fluoride, at the same time XRD measurements did not reveal other phase, except Ag. The electrocatalytic activity of AgNF/GC in electrochemical reduction of a series of substituted bromobenzenes and fluorinated bromoalkanes was notably higher compared to bulk silver. The peak values of the processes, assigned to debromination of the organic bromides by means of DFT calculations, were shifted to positive potentials; however there was no change of the current values of such processes compared to bulk silver. It can be concluded that the

View Article Online
DOI: 10.1039/C8NJ03460E



dehalogenation process occurred on active sites, but not on the whole surface of AgNF. Preparative electrolysis of 1-bromo-4-fluorobenzene on AgNF electrode at the potential of the most positive peak allowed obtaining fluorobenzene with *ca.* 60 % faradaic efficiency. AgNF/GC was also shown to be catalytically active in reduction of alkylbromides – $CF_3CHClBr$ and $CF_2Br_2$; reduction of the first bromide was accompanied with destruction of AgNF, presumable due to formation of soluble complex with alkene – one of possible reaction products. AgNF deterioration upon halothane electrolysis was also confirmed by chronoamperogram measurement.

In our opinion, the results of this study can be used for creation of electrode materials for deterioration of halogen-organic compounds in waste waters, as well as for creation of electrochemical sensors for organic halides detection and analysis. We also see high potential of AgNF use as catalyst of other organic reactions.

**Associated content**

***Supporting information.*** Supporting information is available free of charge at DOI:
CVs used for pseudocapacitance measurements (Fig. S1); microphoto of AgNF/GC subjected to 6 cycles of application and dissolution of paraffin (Fig. S2); low-angle X-ray diffraction patterns of AgNF/GC (Fig. S3); an interpretation of electron diffraction image of the sample of AgNF (Fig. S4); CV of neat electrolyte solution measured on AgNF/GC working electrode. (Fig. S5); Awk script used for slight distortion of molecular geometries before DFT calculations; DFT-calculated energy profiles *vs.* C–Br bond lengths of anion radicals of aryl bromides (Fig. S6); CVs of consequent scans of bromobenzene and halothane solutions on AgNF/GC stirred after each scan. (Fig. S7, S8); $^{19}$F-NMR spectrum of the electrolyte after electrolysis of 1-bromo-4-fluorobenzene on AgNF/GC (Fig S9); DFT-calculated C–Br distances and bond orders of studied organic halides (neutral and reduced species) at the corresponding equilibrium geometries (Table S1); input and output files of the DFT calculations (7zip archive).

**Conflicts of interest**

There are no conflicts of interest to declare.

**Acknowledgements**

S.V.K. thanks to the National Academy of sciences of Ukraine and Enamine Ltd. for support of this study. K.M.A. and B.A.E. thank Russian Academy of science and Federal Agency of Scientific Organizations for support of this study. A.S.L. thanks to M.M.Kurmach and Dr. O.V.Shvets for help in conducting XRD and optical microscopy experiments as well as to Dr. I.E.Kotenko and Dr. I.V.Vasylenko for assistance in TEM measurements. The work was partially funded by Stipend of the National Academy of Sciences of Ukraine for young scientists awarded to A.S.L. in 2017.

View Article Online
DOI: 10.1039/C8NJ03460E





## References


1 L. Liu and A. Corma, *Chem. Rev.*, 2018, **118**, 4981–5079.
2 Y. Liu, G. Zhao, D. Wang and Y. Li, *Natl. Sci. Rev.*, 2015, **2**, 150–166.
3 M. Pérez-Lorenzo, *J. Phys. Chem. Lett.*, 2012, **3**, 167–174.
4 A. Biffis, P. Centomo, A. Del Zotto and M. Zecca, *Chem. Rev.*, 2018, **118**, 2249–2295.
5 D. Nandi, R. U. Islam, N. Devi, S. Siwal and K. Mallick, *New J. Chem.*, 2018, **42**, 812–816.
6 J. Mondal, A. Biswas, S. Chiba and Y. Zhao, *Sci. Rep.*, , DOI:10.1038/srep08294.
7 J. Song, Z.-F. Huang, L. Pan, K. Li, X. Zhang, L. Wang and J.-J. Zou, *Appl. Catal. B Environ.*, 2018, **227**, 386–408.
8 D. Kim, Y. Lee, Y. Kim, K. Mingle, J. Lauterbach, D. A. Blom, T. Vogt and Y. Lee, *Chem. - Eur. J.*, 2018, **24**, 1041–1045.
9 Y. Huang, Z. Liu, G. Gao, G. Xiao, A. Du, S. Bottle, S. Sarina and H. Zhu, *ACS Catal.*, 2017, **7**, 4975–4985.
10 E. C. Dreaden, A. M. Alkilany, X. Huang, C. J. Murphy and M. A. El-Sayed, *Chem Soc Rev*, 2012, **41**, 2740–2779.
11 R. R. Arvizo, S. Bhattacharyya, R. A. Kudgus, K. Giri, R. Bhattacharya and P. Mukherjee, *Chem. Soc. Rev.*, 2012, **41**, 2943.
12 C. Zhu, G. Meng, P. Zheng, Q. Huang, Z. Li, X. Hu, X. Wang, Z. Huang, F. Li and N. Wu, *Adv. Mater.*, 2016, **28**, 4871–4876.
13 M. A. Bhosale and B. M. Bhanage, *Curr. Org. Chem.*, 2015, **19**, 708–727.
14 X.-Y. Dong, Z.-W. Gao, K.-F. Yang, W.-Q. Zhang and L.-W. Xu, *Catal. Sci. Technol.*, 2015, **5**, 2554–2574.
15 C. Wen, A. Yin and W.-L. Dai, *Appl. Catal. B Environ.*, 2014, **160–161**, 730–741.
16 L. Yang, L. Xing, C. Cheng, L. Xia and H. Liu, *RSC Adv.*, 2016, **6**, 31871–31875.
17 G. Vilé, D. Baudouin, I. N. Remediakis, C. Copéret, N. López and J. Pérez-Ramírez, *ChemCatChem*, 2013, **5**, 3750–3759.
18 M. J. Landry, A. Gellé, B. Y. Meng, C. J. Barrett and A. Moores, *ACS Catal.*, 2017, **7**, 6128–6133.
19 S. Rondinini, G. Aricci, Ž. Krpetić, C. Locatelli, A. Minguzzi, F. Porta and A. Vertova, *Fuel Cells*, 2009, **9**, 253–263.
20 A. Minguzzi, O. Lugaresi, G. Aricci, S. Rondinini and A. Vertova, *Electrochem. Commun.*, 2012, **22**, 25–28.
21 D. Koushik, S. Sen Gupta, S. M. Maliyekkal and T. Pradeep, *J. Hazard. Mater.*, 2016, **308**, 192–198.
22 H. Liu, J. Bai, S. Wang, C. Li, L. Guo, H. Liang, T. Xu, W. Sun and H. Li, *Colloids Surf. Physicochem. Eng. Asp.*, 2014, **448**, 154–159.
23 Z. Li, C. Zhang, J. Tian, Z. Zhang, X. Zhang and Y. Ding, *Catal. Commun.*, 2014, **53**, 53–56.
24 K. Seth, S. R. Roy, D. N. Kommi, B. V. Pipaliya and A. K. Chakraborti, *J. Mol. Catal. Chem.*, 2014, **392**, 164–172.
25 R. J. Isaifan, S. Ntais and E. A. Baranova, *Appl. Catal. Gen.*, 2013, **464–465**, 87–94.
26 B. Roldan Cuenya and F. Behafarid, *Surf. Sci. Rep.*, 2015, **70**, 135–187.
27 S. Cao, F. (Feng) Tao, Y. Tang, Y. Li and J. Yu, *Chem. Soc. Rev.*, 2016, **45**, 4747–4765.
28 B. C. Tappan, S. A. Steiner and E. P. Luther, *Angew. Chem. Int. Ed.*, 2010, **49**, 4544–4565.
29 B. Rezaei, M. Mokhtarianpour and A. A. Ensafi, *Int. J. Hydrog. Energy*, 2015, **40**, 6754–6762.
30 S. Sen, D. Liu and G. T. R. Palmore, *ACS Catal.*, 2014, **4**, 3091–3095.
31 B. C. Tappan, M. H. Huynh, M. A. Hiskey, D. E. Chavez, E. P. Luther, J. T. Mang and S. F. Son, *J. Am. Chem. Soc.*, 2006, **128**, 6589–6594.
32 S. Cherevko, X. Xing and C.-H. Chung, *Electrochem. Commun.*, 2010, **12**, 467–470.
33 M. Jin and H. Ma, *Russ. J. Electrochem.*, 2013, **49**, 1081–1085.
34 Q. Lu, J. Rosen, Y. Zhou, G. S. Hutchings, Y. C. Kimmel, J. G. Chen and F. Jiao, *Nat. Commun.*, 2014, **5**, ncomms4242.

View Article Online
DOI: 10.1039/C8NJ03460E



35 M. Ma, B. J. Trześniewski, J. Xie and W. A. Smith, *Angew. Chem. Int. Ed.*, 2016, **55**, 9748–9752.
36 J. Biener, A. M. Hodge, A. V. Hamza, L. M. Hsiung and J. H. Satcher, *J. Appl. Phys.*, 2005, **97**, 024301.
37 M. Hakamada, Y. Chino and M. Mabuchi, *Mater. Lett.*, 2010, **64**, 2341–2343.
38 G.-M. Yang, X. Chen, J. Li, Z. Guo, J.-H. Liu and X.-J. Huang, *Electrochimica Acta*, 2011, **56**, 6771–6778.
39 H.-J. Jin, D. Kramer, Y. Ivanisenko and J. Weissmüller, *Adv. Eng. Mater.*, 2007, **9**, 849–854.
40 S. Eugénio, T. M. Silva, M. J. Carmezim, R. G. Duarte and M. F. Montemor, *J. Appl. Electrochem.*, 2014, **44**, 455–465.
41 D. Ressnig and M. Antonietti, *Chem. Mater.*, 2014, **26**, 4064–4067.
42 A. Dursun, D. V. Pugh and S. G. Corcoran, *J. Electrochem. Soc.*, 2003, **150**, B355.
43 H.-C. Shin, J. Dong and M. Liu, *Adv. Mater.*, 2003, **15**, 1610–1614.
44 E. T. Martin, C. M. McGuire, M. S. Mubarak and D. G. Peters, *Chem. Rev.*, 2016, **116**, 15198–15234.
45 V. Pifferi, G. Facchinetti, A. Villa, L. Prati and L. Falciola, *Catal. Today*, 2015, **249**, 265–269.
46 A. Gennaro, C. M. Sánchez-Sánchez, A. A. Isse and V. Montiel, *Electrochem. Commun.*, 2004, **6**, 627–631.
47 V. E. Titov, A. M. Mishura and V. G. Koshechko, *Theor. Exp. Chem.*, 2011, **46**, 399–408.
48 J. Langmaier and Z. Samec, *J. Electroanal. Chem.*, 1996, **402**, 107–113.
49 A. S. Lytvynenko, R. A. Polunin, M. A. Kiskin, A. M. Mishura, V. E. Titov, S. V. Kolotilov, V. M. Novotortsev and I. L. Eremenko, *Theor. Exp. Chem.*, 2015, **51**, 54–61.
50 A. S. Lytvynenko, S. V. Kolotilov, M. A. Kiskin, O. Cador, S. Golhen, G. G. Aleksandrov, A. M. Mishura, V. E. Titov, L. Ouahab, I. L. Eremenko and V. M. Novotortsev, *Inorg. Chem.*, 2014, **53**, 4970–4979.
51 V. E. Titov, A. M. Mishura and V. G. Koshechko, *Theor. Exp. Chem.*, 2006, **42**, 224–228.
52 E. R. Wagoner and D. G. Peters, *J. Electrochem. Soc.*, 2013, **160**, G135–G141.
53 A. A. Isse, S. Gottardello, C. Maccato and A. Gennaro, *Electrochem. Commun.*, 2006, **8**, 1707–1712.
54 A. Brzózka, A. Jeleń, A. M. Brudzisz, M. M. Marzec and G. D. Sulka, *Electrochimica Acta*, 2017, **225**, 574–583.
55 W. L. F. Armarego, *Purification of laboratory chemicals*, Elsevier/Butterworth-Heinemann, Amsterdam ; Boston, 6th ed., 2009.
56 *Org. Synth.*, 1956, **36**, 46.
57 A. Motheo, S. Machado, M. VanKampen and J. Santos, *J. Braz. Chem. Soc.*, 1993, **4**, 122–127.
58 F. Neese, *Wiley Interdiscip. Rev. Comput. Mol. Sci.*, 2012, **2**, 73–78.
59 J. P. Perdew, K. Burke and M. Ernzerhof, *Phys. Rev. Lett.*, 1996, **77**, 3865–3868.
60 J. P. Perdew, K. Burke and M. Ernzerhof, *Phys. Rev. Lett.*, 1997, **78**, 1396–1396.
61 F. Weigend and R. Ahlrichs, *Phys. Chem. Chem. Phys.*, 2005, **7**, 3297–3305.
62 A. Schäfer, H. Horn and R. Ahlrichs, *J. Chem. Phys.*, 1992, **97**, 2571.
63 F. Neese, *J. Comput. Chem.*, 2003, **24**, 1740–1747.
64 F. Weigend, *Phys. Chem. Chem. Phys.*, 2006, **8**, 1057–1065.
65 V. Barone and M. Cossi, *J. Phys. Chem. A*, 1998, **102**, 1995–2001.
66 S. Grimme, J. Antony, S. Ehrlich and H. Krieg, *J. Chem. Phys.*, 2010, **132**, 154104.
67 S. Grimme, S. Ehrlich and L. Goerigk, *J. Comput. Chem.*, 2011, **32**, 1456–1465.
68 E. R. Johnson and A. D. Becke, *J. Chem. Phys.*, 2006, **124**, 174104.
69 M. D. Hanwell, D. E. Curtis, D. C. Lonie, T. Vandermeersch, E. Zurek and G. R. Hutchison, *J. Cheminformatics*, 2012, **4**, 17.
70 A. K. Rappe, C. J. Casewit, K. S. Colwell, W. A. Goddard and W. M. Skiff, *J. Am. Chem. Soc.*, 1992, **114**, 10024–10035.

View Article Online
DOI: 10.1039/C8NJ03460E

71 N. M. O'Boyle, M. Banck, C. A. James, C. Morley, T. Vandermeersch and G. R. Hutchison, *J. Cheminformatics*, 2011, **3**, 33.
72 A. S. Lytvynenko, S. V. Kolotilov, M. A. Kiskin, I. L. Eremenko and V. M. Novotortsev, *Phys. Chem. Chem. Phys.*, 2015, **17**, 5594–5605.
73 P. Rüetschi and P. Delahay, *J. Chem. Phys.*, 1955, **23**, 195–199.
74 D. Kong, J. J. Cha, H. Wang, H. R. Lee and Y. Cui, *Energy Environ. Sci.*, 2013, **6**, 3553.
75 B. D. Cullity and S. R. Stock, *Elements of X-ray diffraction*, Pearson education limited, Harlow, 2014.
76 V. B. Fenelonov, V. N. Romannikov and A. Y. Derevyankin, *Microporous Mesoporous Mater.*, 1999, **28**, 57–72.
77 R. W. G. Wyckoff, *Crystal Structures*, Wiley, 1963.
78 S. Gražulis, D. Chateigner, R. T. Downs, A. F. T. Yokochi, M. Quirós, L. Lutterotti, E. Manakova, J. Butkus, P. Moeck and A. Le Bail, *J. Appl. Crystallogr.*, 2009, **42**, 726–729.
79 W. Schwieger, A. G. Machoke, T. Weissenberger, A. Inayat, T. Selvam, M. Klumpp and A. Inayat, *Chem. Soc. Rev.*, 2016, **45**, 3353–3376.
80 C. Durante, A. A. Isse, F. Todesco and A. Gennaro, *J. Electrochem. Soc.*, 2013, **160**, G3073–G3079.
81 I. Mayer, *Chem. Phys. Lett.*, 1983, **97**, 270–274.
82 A. A. Isse, P. R. Mussini and A. Gennaro, *J. Phys. Chem. C*, 2009, **113**, 14983–14992.
83 A. A. Isse, L. Falciola, P. R. Mussini and A. Gennaro, *Chem Commun*, 2006, 344–346.

View Article Online
DOI: 10.1039/C8NJ03460E

Nanostructuring of silver notably improved its electrocatalytic activity in reductive dehalogenation of a variety of aryl and alkyl bromides.

View Article Online
DOI: 10.1039/C8NJ03460E



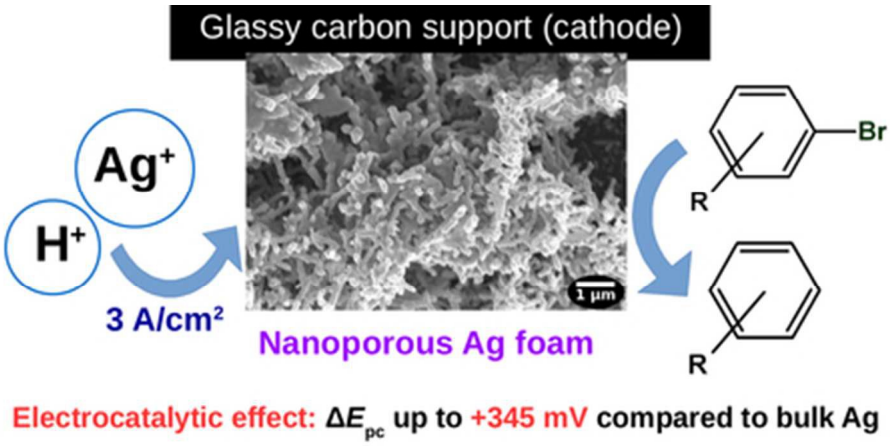


39x19mm (300 x 300 DPI)